Design of a Trench-Assisted Optical Fiber for Generating Bessel Beams With Different Shapes

Nan Wang, Yusheng Liu, Wenjuan Li, Xinwei Huo, Yingchao Liu, and Lei Zhang, *Member, IEEE*

***Abstract*—We have designed a trench-assisted optical fiber that can generate Bessel beams with different shapes in the fundamental mode. The trench-assisted structure is nested by rings with different refractive indexes on the cross-section. The fundamental mode field properties of the trench-assisted fiber are analyzed by using the finite element method. For the wavelengths from 400 nm to 2500 nm, the fundamental modes appear as Bessel beams with different shapes. The zero-order Bessel beams exhibit at the longer wavelength region, and the higher-order Bessel beams show at the shorter wavelength region. The Bessel beams' shape can also be adjusted by tuning the structure parameters on the cross-section of the designed trench-assisted fiber.**

***Index Terms*—Bessel beam, special optical fiber, trench-assisted.**

I. Introduction

OPTICAL imaging technologies have important applications in the fields of biomedicine [1]–[3], computer vision system [4], and industrial testing [5]. Various optical imaging technologies have been developed, such as synthetic aperture imaging [6], optical coherence tomography [7], scanning confocal microscopy [8], and holographic imaging [9]. In the area of biomedical photonics imaging, higher resolution and faster imaging speed are required. Recently, the illumination method with Bessel beams is investigated to improve the imaging systems' performances. Chi Liu et al. stretch the multiphoton microscopy's axial point spread function through Bessel beam illumination [10]. Haydn Martin et al. use the Bessel beam in optical coherence tomography to extend the system's depth of focus [5]. Sota Takanezawa et al. improve light-sheet two-photon microscopy's axial resolution by using Bessel beam illumination [11].

Manuscript received 14 July 2022; accepted 30 July 2022. Date of publication 3 August 2022; date of current version 15 August 2022. This work was supported in part by the Open Fund of State Key Laboratory of Information Photonics and Optical Communications, Beijing University of Posts and Telecommunications, China under Grant IPOC2021B06, and in part by the Basic Scientific Research Funds for Universities in Hebei Province under Grant JQN2021019. *(Corresponding author: Lei Zhang.)*

Nan Wang, Yusheng Liu, Wenjuan Li, Xinwei Huo, and Lei Zhang are with the Key Laboratory for Special Fiber and Fiber Sensor of Hebei Province, School of Information Science and Engineering, Yanshan University, Qinhuangdao 066004, China (e-mail: wann@stumail.ysu.edu.cn; edwardliu@stumail.ysu.edu.cn; lwj@stumail.ysu.edu.cn; huoxinwei@stumail.ysu.edu.cn; zhangl85@ysu.edu.cn).

Yingchao Liu is with the College of Artificial Intelligence, North China University of Science and Technology, Tangshan 063210, China (e-mail: yingchaoliucbb@163.com).

Digital Object Identifier 10.1109/JPHOT.2022.3196094

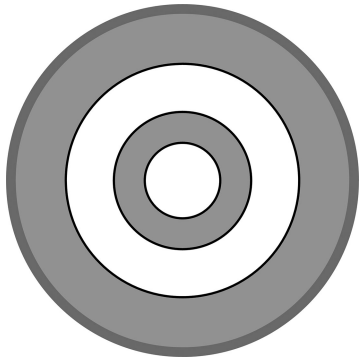

Fig. 1. Cross-sectional structure of the designed optical fiber.

More than 30 years ago, Durnin first got the diffraction-free Bessel beam by solving the Helmholtz equation and generated the zero-order Bessel beam experimentally by using an annular slit [12], [13]. Then, a bunch of ways are explored to generate Bessel beams, such as holography [14], [15], resonant cavity [16], and lens-axicon [17]. Novel fiber technologies also have been proposed to generate Bessel beams, such as fiber grating [18], photonic crystal fiber [19], multimode fiber, and hybrid fiber [20]–[22]. Lee et al. generated a Bessel-like beam using a three-segments integrated fiber. Deng et al. transformed a Gaussian beam into a Bessel-like beam by using a circular array core fiber [20]. Siddharth Ramachandran et al. excited the Gaussian beam to the Bessel beam with a long period fiber grating [18].

To further explore the Bessel beams' advantages, several kinds of methods have been proposed to generate Bessel beams in arbitrary order. Vicente et al. summarized the classification of Bessel beams' electromagnetic fields and concluded a general framework to generate arbitrary order Bessel beams by using hypersurface technology [22]. Xuli Wei et al. generated Bessel beams with any order in the terahertz frequency range by using a 3D printed axicon [17]. In this paper, a trench-assisted optical fiber was designed to generate Bessel beams with different shapes in the fundamental mode.

II. Fiber Structure

The cross-section structure of the designed trench-assisted optical fiber is shown in Fig. 1. Low refractive index or high refractive index trenches distribute around the core on fiber's

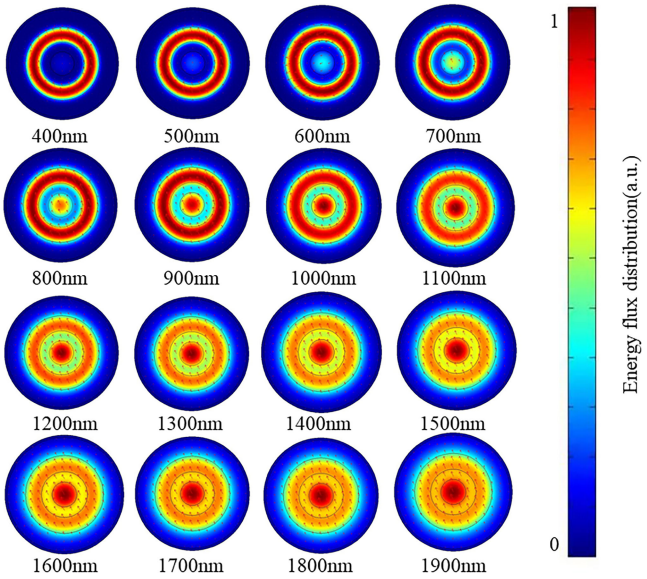

Fig. 2. The evolution of the HE11 mode in the designed optical fiber with wavelengths ranging from 400 nm to 1900 nm.

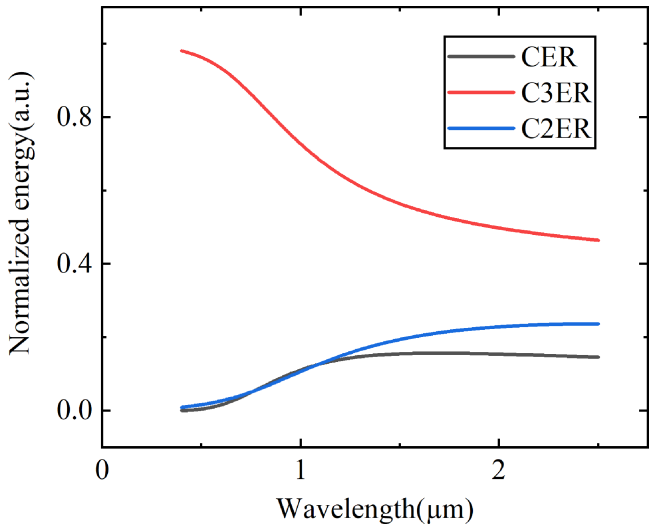

Fig. 3. The evolution of the energy ratios for the regions of C1, C2, and C3 in the fiber cross-section with wavelengths ranging from 400 nm to 2500 nm.

cross-section, which can play an important role in light-filed regulation. The materials with relatively higher and lower refractive index show an interlaced distribution pattern in the cross-section. The white area denotes the material with a higher refractive index of N1 = 1.4457, and the gray area denotes the material with a lower refractive index of N2 = 1.4378. The core is represented by C1, and the second, third, and fourth rings are represented by C2, C3, and C4, respectively. The radius of the core is r1 = 2.75 μm, and the outermost radius of the second, third, and fourth rings are r2 = 5 μm, r3 = 8.5 μm, and r4 = 12.5 μm, respectively.

III. Simulation Results and Discussions

In order to verify that the Bessel beam can be generated by the designed optical fiber, we simulated the fiber's HE11 mode property through the COMSOL Multiphysics software with the finite element method. During the simulations, scattering Trench-assisted boundary conditions are used. Fig. 2 shows the evolution of the fiber's HE11 mode with the wavelength ranging from 400 nm to 1900 nm. The Bessel beams with light fields distributed in rings series can be found. The zero-order Bessel beams with a bright spot at the central part of the ring-shaped mode field appear in the longer wavelength region. The high-order Bessel beams with ring-shaped mode fields appear in the shorter wavelength region. The arrows on the mode field images indicate the direction of the electric field.

The energy distributed on C1, C2, C3, and the whole cross-section regions of the optical fiber is calculated by using the electromagnetic field theory.

$$P = \int_{Sc} \vec{Sav} \cdot d\vec{a} = \int_{Sc} \frac{1}{2} \mathrm{Re}[\vec{E} \times \vec{H^*}] \cdot d\vec{a} \tag{1}$$

where, P represents the average power, $\vec{Sav}$ represents the average energy-flux density, Re[] stands for the real part of the content in brackets, $\vec{E}$ represents the electric field, $\vec{H^*}$ represents the complex conjugate of the magnetic field, $\mathrm{d}\vec{a}$ represents an infinitesimal area vector, and the integral is over C1, C2, C3, or the whole cross-section region of the optical fiber. Because the ratio of the average power is the same as the ratio of the average energy crossing the defined field, the core energy ratio (CER) is defined as the ratio between the average power in the core region and the average power in the whole cross-section of the fiber.

$$CER = \frac{P\mathrm{core}}{P\mathrm{overall}} \tag{2}$$

Similarly, the average power in C2 and C3 regions can be divided by the average power in the whole cross-section of the fiber, then the C2 energy ratio (C2ER) and C3 energy ratio (C3ER) can be obtained. For the designed fiber with cross-section parameters of r1 = 2.75 μm, r2 = 5 μm, r3 = 8.5 μm, and r4 = 12.5 μm, the evolutions of CER, C2ER, and C3ER versus the wavelength ranging from 400 nm to 2500 nm are shown in Fig. 3. The evolution curves of C3ER, C2ER, and CER in Fig. 3 are distinguished by red, blue, and black, respectively. In the overall wavelengths from 400 nm to 2500 nm, the two curves of CER and C2ER rise violently in the early stage, rise gently in the middle stage, and tend to be stable after 1500 nm in the later stage. C3ER decreases violently in the early stage and decreases gently in the later stage. In the short wavelength region below 500 nm, the C3ER is much higher than the other two curves, especially at 400 nm, the C3ER is 98% which is very close to 1. This shows that the energy is mainly concentrated in the high refractive index ring C3. The high-order Bessel beam with a ring-shaped mode field is generated. In the wavelength region over 1500 nm, the sum of CER and C2ER is close to 50%, and the C3ER has declined to 46% at 2500 nm. It shows that a substantial part of the energy distributes in the core region, and the zero-order Bessel beam is generated.

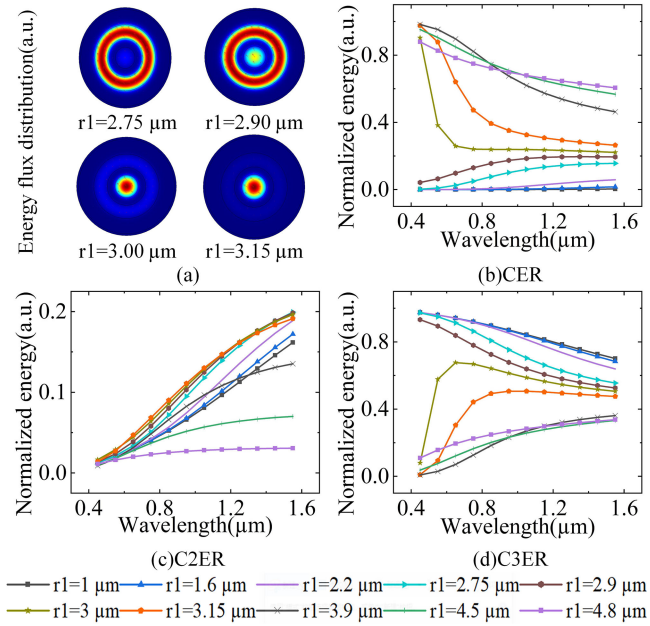

Fig. 4. (a) The HE11 mode fields at 450 nm for r1 = 2.75 μm, 2.90 μm, 3.00 μm, and 3.15 μm; (b) CER diagram, (c) C2ER diagram, and (d) C3ER diagram for r1 varying from 1 μm to 4.8 μm.

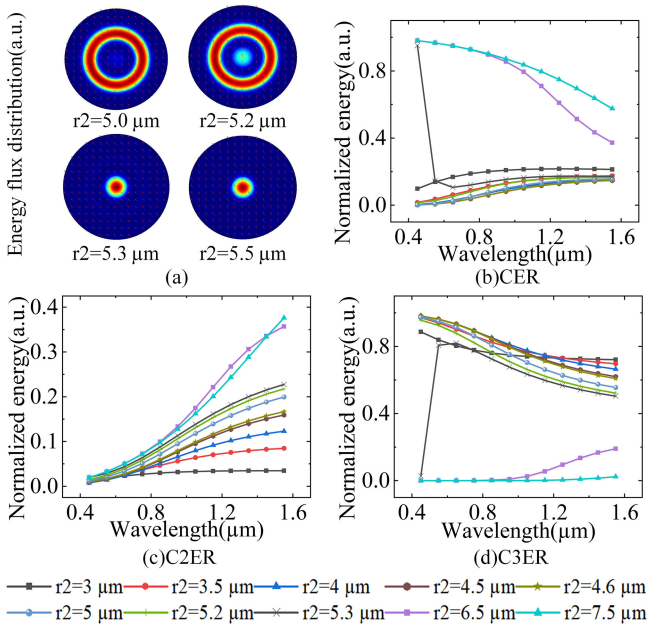

Fig. 5. (a) The HE11 mode fields at 450 nm for r2 = 5.0 μm, 5.2 μm, 5.3 μm, and 5.5 μm; (b) CER diagram, (c) C2ER diagram, and (d) C3ER diagram for r2 varying from 3 μm to 7.5 μm.

Then, the evolutions of the energy ratios are systematically investigated by adjusting the parameters of the cross-sectional structure of the trench-assisted fiber. For the case of r2 = 5.0 μm, r3 = 8.5 μm, r4 = 12.5 μm, and the core radius r1 is set at 1 μm, 1.6 μm, 2.2 μm, 2.75 μm, 2.9 μm, 3 μm, 3.15 μm, 3.9 μm, 4.5 μm, and 4.8 μm respectively, the evolutions of the energy ratios for CER, C2ER, and C3ER with the wavelength increasing from 450 nm to 1550 nm are shown in Fig. 4(b)–(d) respectively. The HE11 mode fields at 450 nm for r1 = 2.75 μm, 2.90 μm, 3.00 μm, and 3.15 μm are shown in Fig. 4(a). While r1 is less than 2.9 μm, the Bessel beams can be generated. When r1 is greater than 3.0 μm, it becomes difficult to generate Bessel beams with the structure. The CER and C3ER curves in Fig. 4(b) and (d) have a sudden change with r1 varying from 2.9 μm to 3.0 μm. For the cases of r1 $\leq$ 2.9 μm, the trends of the CER, C2ER, and C3ER curves in Fig. 4 are the same as those in Fig. 3. With the increase of r1 from 1 μm to 2.9 μm, the energy in the ring region declines, and the energy in the core region raises. This is because a relatively larger core can provide stronger confinement to the light field. When r1 $\geq$ 3.0 μm, the trends of the curves in Fig. 4 are opposite to that in Fig. 3. With the further increase of r1, the area of the C2 region becomes smaller and smaller, and the light field is difficult to be regulated to generate Bessel beams by the trench-assisted structure. The energy ratios of the Bessel beams at different cross-section parts of the fiber also can be widely tuned by adjusting the wavelength. For example, when r1 is 2.5 μm, with the wavelength tuned from 450 nm to 1550 nm, the CER energy ratio increases from 0.01% to 10.3%, the C2ER energy ratio raises from 1.25% to 19.67%, and the C3ER energy ratio declines from 97.5% to 59.8%. This shows that at the shorter wavelength region more energy can be concentrated in the C3 high refractive index ring. This is because the numerical aperture for the shorter wavelength is relatively larger, and the light is relatively easy to spread into the high refractive ring in the cross-section of the fiber.

For the case of r1 = 2.75 μm, r3 = 8.5 μm, r4 = 12.5 μm, and the r2 is set at 3 μm, 3.5 μm, 4 μm, 4.5 μm, 4.6 μm, 5 μm, 5.2 μm, 5.3 μm, 6.5 μm, and 7.5 μm respectively, the evolutions of the energy ratios for CER, C2ER, and C3ER, with the wavelength increasing from 450 nm to 1550 nm, are shown in Fig. 5(b)–(d) respectively. C2ER increases and C3ER decreases, at each specified wavelength when r2 is increased from 4 μm to 5.2 μm. And the corresponding CER decreases with the r2 increasing from 4 μm to 4.6 μm, and then increases with the r2 increasing from 4.6 μm to 5.2 μm. The CER curves of r2 = 4.5 μm and r2 = 4.6 μm almost coincides. Bessel beams can be generated in the above radius range. With r2 changing from 5.2 μm to 5.3 μm, CER increases from 1.5% to 95% at 450 nm, and the corresponding C3ER drops from 96% to 2.9%. This analysis is consistent with the HE11 mode fields at 450 nm for r2 = 5.0 μm, 5.2 μm, 5.3 μm, and 5.5 μm in Fig. 5(a). The concentration region of energy changes from ring to core, and it is difficult to generate Bessel beams. When r2 is increased from 5.3 μm to 7.5 μm, CER increases, and C3ER decreases at each specified wavelength. CER decreases from about 100%, and C3ER gradually increases from about 0% with the wavelength ranging from 450 nm to 1550 nm, it is also difficult to generate Bessel beams. Obviously, the generation of Bessel beams is affected by r2, and the increase of r2 means that the area of the low refractive index region decreases. Consequently, the narrow low refraction region is difficult to play the role of light field regulation. When r2 is increased from 3 μm to 4 μm, CER decreases, C2ER and C3ER increase, at each specified wavelength. This is because a wider low refractive region prevents the light field energy from

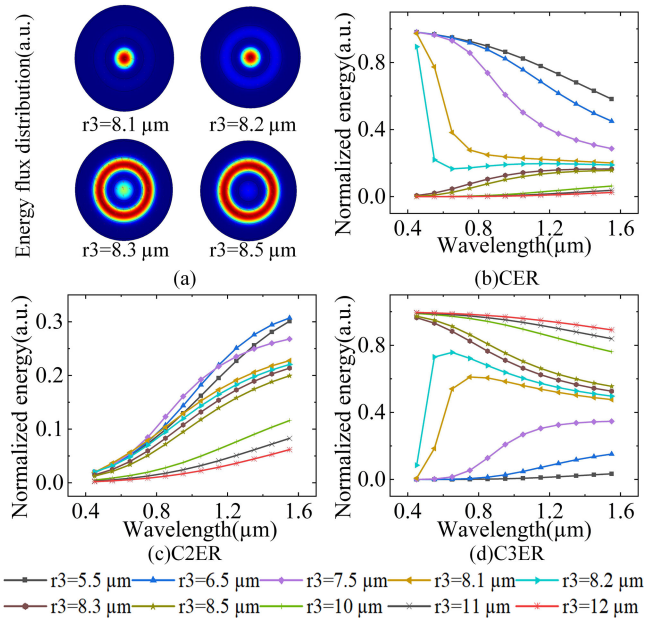

Fig. 6. (a) The HE11 mode fields at 450 nm for r3 = 8.1 μm, 8.2 μm, 8.3 μm, and 8.5 μm; (b) CER diagram, (c) C2ER diagram, and (d) C3ER diagram for r3 varying from 5.5 μm to 12 μm.

spreading to the C3 ring, which leads to most of the energy being bound in the core.

For the case of r1 = 2.75 μm, r2 = 5.0 μm, r4 = 12.5 μm, the r3 is set at 5.5 μm, 6.5μm, 7.5 μm, 8.1 μm, 8.2 μm, 8.3 μm, 8.5 μm, 10 μm, 11 μm, and 12 μm respectively, the evolutions of the CER, C2ER and C3ER energy ratios versus the wavelength are shown in Fig. 6(b)–(d) respectively. When r3 is increased from 8.3 μm to 12 μm, CER and C2ER decrease, and C3ER increases, at each specified wavelength. CER gradually increases from about 0%, and C3ER gradually decreases from about 100% with the wavelength ranging from 450 nm to 1550 nm. As r3 is in the range of 8.3 μm-12 μm, C3ER decreases to 52.6% at the wavelength of 1550 nm, and Bessel beams can still be generated under this condition. That's because the wider high refraction C3 ring can promote the propagation of light energy from the fiber core to the C3 ring. Drastic change at the short wavelength edge appears near the point of r3 = 8.2 μm. This also can be observed from the HE11 mode fields at 450 nm for r3 = 8.1 μm, 8.2 μm, 8.3 μm, and 8.5 μm in Fig. 6(a). When r3 is increased from 5.5 μm to 8.2 μm, CER gradually decreases from about 100%, and C3ER gradually increases from about 0% with the wavelength increasing from 450 nm to 1550 nm. Bessel beams are difficult to be generated in the circumstances. Because the light energy is difficult to be constrained in the narrow high refractive C3 ring.

These evolution curves reflect that the energy ratios is significantly related to the cross-section structure of the designed optical fiber. No matter which parameter is changed, the CER, C2ER, and C3ER energy ratios will be affected. The increases of r2 and r3 have opposite effects on the evolutional trends of the energy ratios for generating of the Bessel beams' range. Fig. 7 shows the HE11 mode fields at 600 nm for r2 = 5.0 μm, r3 = 8.5 μm, r4 = 12.5 μm, and r1 increasing from 2.7 μm to 3.05 μm.

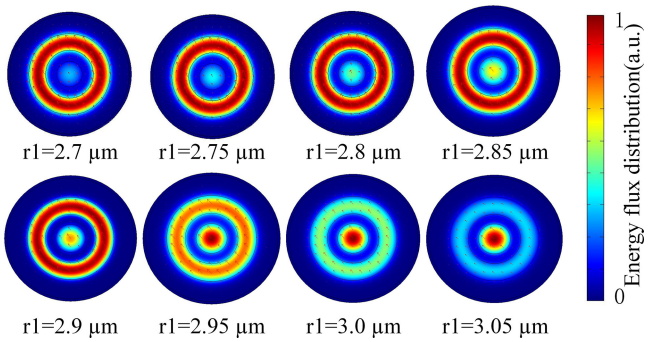

Fig. 7. The distributions of the fundamental mode field at 600 nm with r1 tuning from 2.7 μm to 3.05 μm.

With the increase of r1, the energy gradually concentrates from the C3 ring to the core region. It reflects that the Bessel beam's shape at a defined wavelength can also be adjusted by tuning the cross-section parameter of the designed trench-assisted fiber.

IV. Conclusion

In conclusion, a trench-assisted optical fiber has been designed to generate Bessel beams with different shapes. The cross-section structure of the trench-assisted optical fiber includes two low refractive index rings and a high refractive index ring, which are concentric and surround the core. The HE11 mode fields are calculated for the wavelengths from 400 nm to 1900 nm. For the longer wavelength, more energy is concentrated in the core region. When the wavelength decreases from 2500 nm to 400 nm, the energy ratio in the high index ring increases from 46% to 98%, and the zero-order Bessel beam are converted to the higher-order Bessel beam. For a fixed wavelength, the Bessel beam's shape can also be changed by adjusting the structure parameters of the trench-assisted optical fiber. In a word, Bessel beams with different shapes can be generated in the trench-assisted optical fiber.

References

[1] D. Sheyn et al., "Bone-chip system to monitor osteogenic differentiation using optical imaging," *Microfluidics Nanofluid*, vol. 23, no. 8, Jul. 2019, Art. no. 99, doi: 10.1007/s10404-019-2261-7.

[2] H. Mostafavi, L. Ghassemifard, A. Rostami, M. Alipour, and S. Nadri, "Trabecular meshwork mesenchymal stem cell transplantation improve motor symptoms of parkinsonian rat model," *Biologicals*, vol. 61, pp. 61–67, Sep. 2019, doi: https://doi.org/10.1016/j.biologicals.2019.06.006.

[3] D. D. Chen et al., "Bright polymer dots tracking stem cell engraftment and migration to injured mouse liver," *Theranostics*, vol. 7, no. 7, pp. 1820–1834, Jun. 2017, doi: 10.7150/thno.18614.

[4] H. Sun, K. J. Kuchenbecker, and G. Martius, "A soft thumb-sized vision-based sensor with accurate all-round force perception," *Nature Mach. Intell.*, vol. 4, no. 2, pp. 135–145, Feb. 2022, doi: 10.1038/s42256-021-00439-3.

[5] H. Martin, P. Kumar, A. Henning, and X. Q. Jiang, "Extended sub-surface imaging in industrial OCT using 'non-diffracting' Bessel beams," *CIRP Ann.*, vol. 69, no. 1, pp. 493–496, May 2020, doi: https://doi.org/10.1016/j.cirp.2020.04.017.

[6] W.-C. Chien, D. S. Dilworth, E. Liu, and E. N. Leith, "Synthetic-aperture chirp confocal imaging," *Appl. Opt.*, vol. 45, no. 3, pp. 501–510, Jan. 2006, doi: 10.1364/AO.45.000501.

[7] D. M. Sampson, A. M. Dubis, F. K. Chen, R. J. Zawadzki, and D. D. Sampson, "Towards standardizing retinal optical coherence tomography angiography: A review," *Light: Sci. Appl.*, vol. 11, no. 1, Mar. 2022, Art. no. 63, doi: 10.1038/s41377-022-00740-9.

[8] P. Stachelek, L. MacKenzie, D. Parker, and R. Pal, "Circularly polarised luminescence laser scanning confocal microscopy to study live cell chiral molecular interactions," *Nature Commun.*, vol. 13, no. 1, Jan. 2022, Art. no. 553, doi: 10.1038/s41467-022-28220-z.

[9] O. A. Sapozhnikov, S. A. Tsysar, V. A. Khokhlova, and W. Kreider, "Acoustic holography as a metrological tool for characterizing medical ultrasound sources and fields," *J. Acoust. Soc. Amer.*, vol. 138, no. 3, pp. 1515–1532, Feb. 2016, doi: 10.1121/1.4928396.

[10] C. Liu et al., "High-speed, multi-modal, label-free imaging of pathological slices with a Bessel beam," *Biomed. Opt. Exp.*, vol. 11, no. 5, pp. 2694–2704, May 2020, doi: 10.1364/BOE.391143.

[11] S. Takanezawa, T. Saitou, and T. Imamura, "Wide field light-sheet microscopy with lens-axicon controlled two-photon Bessel beam illumination," *Nature Commun.*, vol. 12, no. 1, May 2021, Art. no. 2979, doi: 10.1038/s41467-021-23249-y.

[12] J. Durnin, J. J. Miceli, and J. H. Eberly, "Diffraction-free beams," *Phys. Rev. Lett.*, vol. 58, no. 15, pp. 1499–1501, Apr. 1987, doi: 10.1103/PhysRevLett.58.1499.

[13] J. Durnin, "Exact solutions for nondiffracting beams. I. The scalar theory," *J. Opt. Soc. Amer. A*, vol. 4, pp. 651–654, Apr. 1987, doi: 10.1364/JOSAA.4.000651.

[14] N. Chattrapiban, E. A. Rogers, D. Cofield, W. T. R. Hill, and R. Roy, "Generation of nondiffracting Bessel beams by use of a spatial light modulator," *Opt. Lett.*, vol. 28, no. 22, pp. 2183–2185, Nov. 2003, doi: 10.1364/OL.28.002183.

[15] S. H. Tao, W. M. Lee, and X. C. Yuan, "Experimental study of holographic generation of fractional Bessel beams," *Appl. Opt.*, vol. 43, no. 1, pp. 122–126, Jan. 2004, doi: 10.1364/AO.43.000122.

[16] A. J. Cox and D. C. Dibble, "Nondiffracting beam from a spatially filtered Fabry–Perot resonator," *J. Opt. Soc. Amer. A*, vol. 9, no. 2, pp. 282–286, Feb. 1992, doi: 10.1364/JOSAA.9.000282.

[17] X. L. Wei et al., "Generation of arbitrary order Bessel beams via 3D printed axicons at the terahertz frequency range," *Appl. Opt.*, vol. 54, no. 36, pp. 10641–10649, Dec. 2015, doi: 10.1364/AO.54.010641.

[18] P. Steinvurzel, K. Tantiwanichapan, M. Goto, and S. Ramachandran, "Fiber-based Bessel beams with controllable diffraction-resistant distance," *Opt. Lett.*, vol. 36, no. 23, pp. 4671–4673, Nov. 2011, doi: 10.1364/OL.36.004671.

[19] C. Xie et al., "High power femtosecond Bessel-X pulses directly from a compact fiber laser system," *Appl. Phys. Lett.*, vol. 101, no. 15, Sep. 2012, Art. no. 151111, doi: 10.1007/s10404-019-2261-7.

[20] H. C. Deng et al., "Circular Airy beam shaping by annular arrayed-core fiber," *J. Lightw. Technol.*, vol. 37, no. 18, pp. 4844–4850, Sep. 2019, doi: 10.1063/1.4758687.

[21] S. R. Lee, J. Kim, S. Lee, T. M. Jung, J. K. Kim, and K. Oh, "All-silica fiber Bessel-like beam generator and its applications in longitudinal optical trapping and transport of multiple dielectric particles," *Opt. Exp.*, vol. 18, no. 24, pp. 25299–25305, Aug. 2010, doi: 10.1364/OE.18.025299.

[22] O. C. Vicente and C. Caloz, "Bessel beams: A unified and extended perspective," *Optica*, vol. 8, no. 4, pp. 451–457, Apr. 2021, doi: 10.1364/OPTICA.411887.